Surface plasmon polariton phase retrieval via nanoscale surface roughness induced cross-polarization scattering

É. McClean-Ilten, J. Gordon, and D. Zerulla*

School of Physics, Science Centre North, University College Dublin, Belfield, Dublin 4, Ireland

(Received 15 November 2021; revised 7 May 2022; accepted 17 May 2022; published 9 June 2022)

This article demonstrates an elegant method for experimental retrieval of the buried phase information of optical phenomena at metallic-dielectric interfaces, especially surface plasmon polaritons (SPP), employing a model explicitly based on roughness-induced cross-polarization scattering. This inherent roughness of the interfaces within typical SPP Attenuated Total Reflection (ATR) setups leads to two interlinked phenomena: Angular broadening and cross-polarization scattering. The microscopic interface features generate altered polarization vectors which are comparably weak but, because of their orthogonal polarization direction, appreciable within the specularly reflected light. The information contained in this s-polarized light enables us to retrieve the phase information of SPPs through the interference model of cross-polarization scattering described here. On that basis, this article demonstrates the retrieval of phase shifts for multiple silver thicknesses of SPPs generated within an ATR geometry. Additionally, the method permits the evaluation of surface roughness parameters, characterization of the angular broadening of reflection, and determination of the thicknesses of the metallic layers.

DOI: 10.1103/PhysRevB.105.235413

I. INTRODUCTION

Surface plasmon polaritons (SPPs) are resonant longitudinal surface charge-density oscillations accompanied by electromagnetic near fields which are confined to the interface of two materials with dielectric constants of opposite signs, i.e., a metal and a dielectric. The excitation of an SPP via an external light source can be achieved through manipulation of the initial momentum of the incoming light. This can be accomplished through various methods including structuring the metallic surface with a grating or specific nanostructure; more commonly the technique of attenuated total internal reflection (ATR) is utilized by transmitting the light through a high refractive index material. Typically a thin metallic film is illuminated by a transverse magnetic (*p*-polarized) electromagnetic radiation incident from a high refractive index medium, as in prism coupling geometries such as the Kretschmann configuration [1]. SPPs excited in this way are extremely sensitive to local refractive index changes owing to exponentially decaying fields into both bounding media and are inferred by the presence of a sudden decrease in the metal reflectivity under optimal conditions. These phenomena have been employed as the basis for optical sensors in real time chemical and biomolecular interaction analysis studies [2]. SPPs also play a significant role in an array of modern applications, such as surface-enhanced raman scattering [3], surface plasmon-coupled emission [4], surface plasmon resonance (SPR) [5,6], and subwavelength optics [7].

In the past decade, there have been a number of publications which report that by measuring the angular dependence of the phase shift due to SPP excitation and not the changes in reflection intensity, an additional two to three orders of magnitude in sensitivity can be achieved [8–11]. However, these are still a relatively small number of publications compared with traditional SPP sensing techniques. This may be due to the complexity of detection which usually involves precise heterodyne setups [12] and algorithms [13] as a consequence of direct phase detection at optical frequencies (10^{15} Hz) not being possible. Therefore interferometric methods of phase measurement resolve into intensity measurements which are, by comparison, easily sensed with photodiodes, photomultiplier tubes, and charge-coupled devices [14]. The improved sensitivity of phase-based measurements is due to a more abrupt angular dependence when compared with the intensity decrease of standard reflection intensity signals [15,16]. Phase-sensitive SPR sensors are also inherently more suitable for SPP imaging [17,18].

In the following we elaborate on an elegant method to recover the phase information based on a self-referencing single beam technique [19]. This technique is characteristically different in terms of design simplicity when compared with optical heterodyne, polarimetry [11], and interferometric techniques recently reviewed by Huang *et al.* [20] and polarization conversion techniques with incident *s* and *p* components [21]. The technique demonstrates that the SPP phase information can be determined solely from the precise measurement of low intensity *s*-polarized light within the reflection channel of an ATR setup with exact incident *p*-polarized light. This technique can be foreseen to be of interest to all SPR-related sensor applications as a melioration to regular amplitude-sensitive systems.

The model of cross-polarization scattering presented here during SPP excitation and subsequent interference of two

*Dominic.Zerulla@ucd.ie

 ©2022 American Physical Society

different channels fully explains the origin of the measured line shape associated with the SPR phase shift, which is buried in the intensity information of the reflected light in an ATR setup. Through rejecting the regularly reflected p-polarized light, which contains the typical SPR characteristics, it is possible to uncover the hidden SPR phase shift-dependent s-polarization components. The model predicts the metal thickness dependence of such a signal through a combination of cross-polarization scattering and interference theories. Specifically, the detected signal depends on two phase-shifted channels of s-polarization in the specular reflection direction, both channels resulting from the phenomenon of cross-polarization scattering within the ATR setup.

The Fresnel equations and Malus' law dictate that in an ideal system there should be no s-polarization component when there is strictly p-polarized incident light entering the system. However, precise measurement of the low intensity s-polarization reflected light in the ATR configuration reveals a nonzero line shape which is characteristically different in terms of shape from the regular SPR reflectivity dip [1] and the polarization conversion "resonant maximum" observed by Elston and Sambles when both s and p components are incident [21].

II. THEORETICAL CONSIDERATIONS

Most optical models of reflection assume the surfaces involved are perfectly smooth, for instance, the Fresnel equations. This assumption holds for macroscopic processes where surface features can be relatively small when compared with the light beam diameter. However, when working on the nanoscale the surface geometry of any optical component will play a significant role in experimental results. Traditionally, atomic force microscopy (AFM) is utilized to determine an average RMS roughness value for a surface. However, from an optical standpoint it is useful to have specific knowledge of the region illuminated by the light source, e.g., a laser. In particular, when performing optical experiments that are sensitive to surface roughness it is desirable to know the surface roughness at the exact point of incidence/reflection. As performing AFM measurements requires removing the sample from the optical system, obtaining the surface characteristics of the exact point of incidence is difficult and time consuming.

Surface roughness can lead to an overall broadening of the reflectivity signal from a system. This is due to the distribution of incident angles experienced at the point of reflection. Such a distribution is directly related to the slope at each point along the surface; see Fig. 1(b). Therefore a measure of this broadening will yield direct information about the roughness at the point of incidence.

For the derived model here, the uniformly coated surfaces are assumed to be homogeneous and isotropic, with a Gaussian surface-height distribution [22]. Consequently the assumption can be made that an incident laser beam illuminating such a surface will experience a Gaussian-distributed range of incident angles. Due to the sharp angular selection of an SPP excitation it is a perfect example to see this broadening directly. It should be noted that, while a Gaussian roughness distribution is often used in the literature including the presented research here, more sophisticated models can be employed which describe the actual roughness of a surface more precisely [23,24]. Such sophisticated models may also benefit from detailed measurements that measure the surface roughness [24]. However, the model presented here is fully informed by the implicitly measured cross-polarization probability. In this context a Gaussian roughness model is fully sufficient to extract all data from the laser excitation.

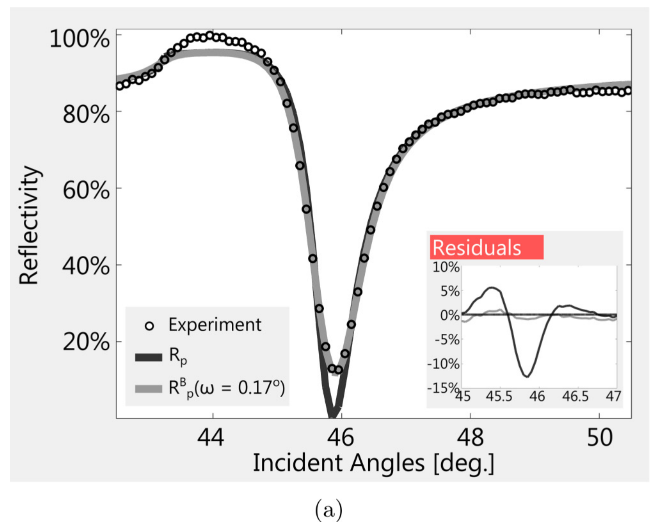

(a)

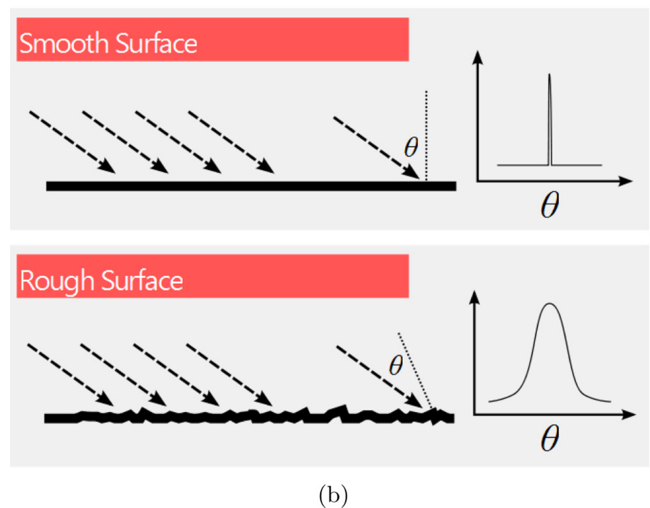

(b)

FIG. 1. Surface roughness effects on the incident angle. (a) Sample 1 data showing comparison of a smooth surface simulation of reflectivity from a Kretschmann configuration setup, R_p, with a Gaussian-broadened simulation, $R^B_p(\omega = 0.17^\circ)$. The insert compares the corresponding residuals of both models; (b) infographic illustrating the effect surface features have on the distribution of incident angles.

The angular selectivity of such an excitation will be on the order of $\pm 0.5^\circ$. Figure 1(a) shows the use of the Fresnel equations to predict the reflectivity, $R_n(\theta)$, from a Kretschmann configuration using 50 nm of silver on a fused silica prism (where $n \in \{p, s\}$ indicates the incident polarization). By introducing a Gaussian distribution around each incident angle (width, $\omega = 0.17^\circ$), contributions from the neighboring angles can be shown to broaden the simulated signal, $R^B_n(\omega, \theta)$; see Eq. (1). The width of the Gaussian is used as a free parameter

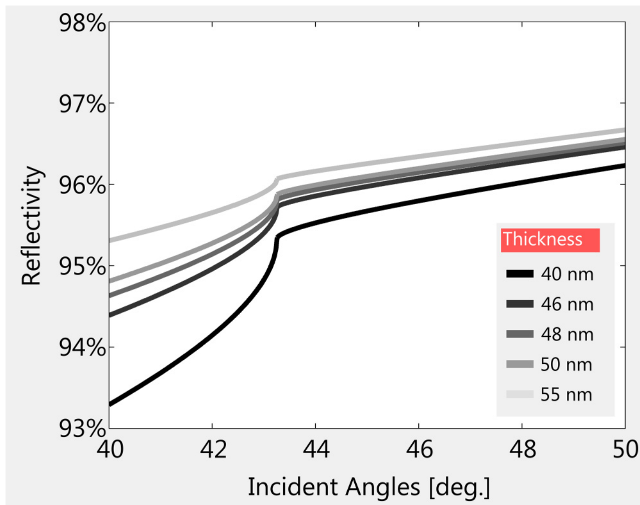

FIG. 2. Simulated s-polarized reflectivity angular scan for various Ag metal thickness: 40, 46, 48, 50, and 55 nm with an excitation wavelength of $\lambda = 561.2$ nm.

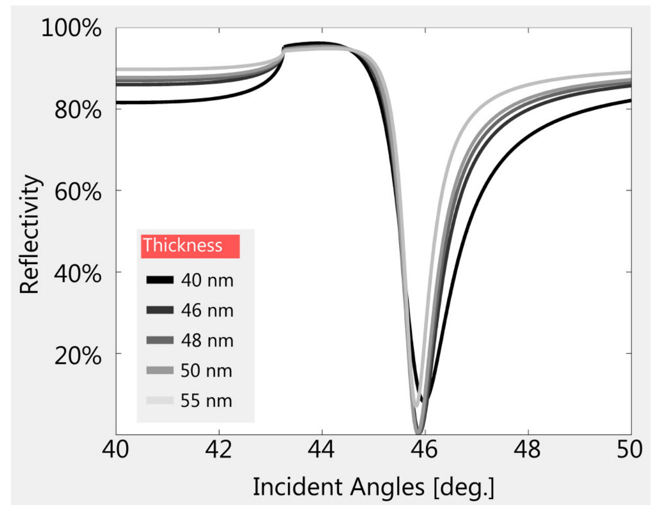

FIG. 3. Simulated p-polarized reflectivity angular scan for various Ag metal thickness: 40, 46, 48, 50, and 55 nm with an excitation wavelength of $\lambda = 561.2$ nm.

when the experimental data are fit by the model. The assertion of the width of the Gaussian provides insightful information about the distribution of true incident angles within the laser spot,

$$R_n^B(\omega, \theta) = \int_{\theta-\frac{\omega}{2}}^{\theta+\frac{\omega}{2}} \frac{R_n(\theta')}{2\pi\omega} \exp\left(-\frac{(\theta'-\theta)^2}{2\omega^2}\right) \mathrm{d}\theta'. \quad (1)$$

Surface roughness in an optical experiment not only effects the angular distribution of the light but also changes the polarization of the light on reflection. This is particularly apparent during the excitation of SPPs. As previously mentioned, in order to excite an SPP the incident light must be polarized parallel to the plane of incidence (p polarized). Classical theories of reflection and polarization predict that after reflection from a Kretschmann configuration all light that was originally p polarized will retain this polarization. The Fresnel equation predictions, i.e., for flat surfaces, for both the reflectivity of s-polarized $R_s(\theta)$ and the p-polarized $R_p(\theta)$ incident light orientations are shown in Figs. 2 and 3, respectively. However, as a consequence of surface roughness, a portion of this light is scattered and results in a polarization conversion to s-polarization, i.e., polarized perpendicular to the plane of incidence. This process is referred to as cross-polarization scattering and can be measured and quantified by the cross-polarization ratio, $C_{p\to s}$; this is the ratio of the intensity of light seen in the perpendicular channel (s polarized) to the intensity of light seen in the original polarization direction (p polarized). As both variables can be measured without significantly altering the system, specifically by changing only the angle of the polarizer, this ratio can be determined experimentally for every angular scan. $C_{p\to s}$ yields information in relation to the average shape and size distribution of features along the surface [22,25].

The SPP excitation condition along a metal surface is achieved by altering the k-vector of the incident light until it satisfies the SPP dispersion relation. The Kretschmann configuration accomplishes this by using a higher index optical material to alter the momentum of the incoming light before it reaches the metallic surface. Here the configuration consists of a semicylindrical glass prism (typically BK7 or fused silica) with a thin layer of metal (on the order of 50 nm) on the flat face. At a specific angle the internal reflection from the prism/metal interface creates the conditions needed for the light to resonantly couple to the free electrons in the metal and therefore excite an SPP. A significant consequence of such coupling is an angular-dependent phase shift between the incoming light and the light measured in the specular reflection direction. As mentioned above, this phenomenon is utilized in biosensors and refractive index retrieval devices. As will be shown in the following, precise and simple measurement of the SPP phase shift, ϕ, is achievable through the process of cross-polarization scattering combined with the Gaussian-broadened model of reflection.

Cross-polarization scattering causes an element of the reflected light to contain an s-polarized component. There are two origins of the s-polarized light in such a system: (a) Cross-polarization scattering of directly reflected light and (b) cross-polarization scattering into the far field subsequent to SPP excitation, the first of which occurs when incident p-polarized light experiences cross-polarization scattering from roughness along the reflecting surface. This contribution can undergo multiple-scattering processes, resulting in an s-polarization signal along the specular reflection direction. This is referred to as direct cross-polarization scattering because it has an immediate effect on the polarization in that all directly cross-polarized light no longer contributes to the excitation of an SPP; it will behave similarly to light which originally entered as s polarized. The intensity profile, I_s^{scat}, of such a channel can be deemed to be proportional to the intensity given by the Gaussian-broadened Fresnel reflectivity for s-polarized light entering the system; see Fig. 2. If I_p^{inc} is the initial laser intensity the intensity of this channel is

given by

$$I_s^{\text{scat}}(\theta) \propto I_p^{\text{inc}} \int_{\theta-\frac{\omega}{2}}^{\theta+\frac{\omega}{2}} \frac{R_s(\theta')}{2\pi\omega} \exp\left(-\frac{(\theta'-\theta)^2}{2\omega^2}\right) \mathrm{d}\theta'. \quad (2)$$

As the incident angle approaches the regime of SPP excitation, the nondirect cross-polarization-scattered portion of the incident p-polarized light will contribute toward the excitation of the SPP. This is commonly detected as a decrease in reflection intensity of the p-polarized light itself. Due to the nature of cross-polarization scattering this light will intrinsically cause an element of s-polarized light, I_s^{spp}. This component is proportional to the intensity given by the Gaussian-broadened Fresnel reflectivity for p-polarized light entering the system, R_p^B; see Fig. 3. From here Eq. (2) can be rearranged to form

$$I_s^{\text{spp}}(\theta) \propto I^{\text{inc}} \int_{\theta-\frac{\omega}{2}}^{\theta+\frac{\omega}{2}} \frac{R_p(\theta')}{2\pi\omega} \exp\left(-\frac{(\theta'-\theta)^2}{2\omega^2}\right) \mathrm{d}\theta'. \quad (3)$$

A typical example for the existence and generation of cross-polarization radiation subsequent to SPP generation is the so-called ATR cone whose origins and polarization behavior are explained in detail by Isfort *et al.* [26,27]. Further examples include scattering of SPPs at mesoscopic structures [28].

The superposition of the above two phase-shifted cross-polarized contributions, Eqs. (2) and (3), results in an angularly dependent s-polarized signal, $I_s(\theta)$ [19],

$$I_s(\theta) = I_s^{\text{scat}} + I_s^{\text{spp}} + 2\cos\left(\phi_s^{\text{spp}} - \phi_s^{\text{scat}}\right)\sqrt{I_s^{\text{scat}} I_s^{\text{spp}}}. \quad (4)$$

The proportionality constant for both Eqs. (2) and (3) is given by the probability of cross-polarization scattering to occur, referred to as $C'_{p\to s}$, which is measured at a fixed angle away from polarization-dependent effects, i.e., some degrees from the SPP excitation angle,

$$C'_{p\to s} = \frac{I_s(\theta)}{\sqrt{(I_p(\theta))^2 + (I_s(\theta))^2}}. \quad (5)$$

As both contributions to Eq. (4) are coherent and are of the same order of magnitude, the profile of this signal is strongly dependent on the phase shift between the channels, $\phi = \phi_s^{\text{spp}} - \phi_s^{\text{scat}}$. This enables the retrieval of phase information from, for example, a standard Kretschmann configuration via two direct measurements: The intensity of the p-polarized component, $I_p(\theta)$ (a standard SPP scan), and the intensity of the s-polarized component, $I_s(\theta)$.

As outlined above, the surface roughness-induced Gaussian broadening can be measured via the original p-polarized SPP scan, $I_p(\theta)$. This provides a value for the Gaussian width, ω, in Eqs. (2) and (3). Once the degree of broadening is known, both $R_s(\theta)$ and $R_p(\theta)$ can be simulated and $R_s^B(\theta)$ and $R_s^B(\theta)$ can be calculated. The precise angular width of the features seen in $I_s(\theta)$ can thus be predicted by the model, allowing for intensity variations over a narrow angular range to equate back to local refractive index changes and for measurements of the phase shift due to the SPP.

Rearranging Eq. (4) and incorporating both measured variables, I_s^{scat} and I_s^{spp}, results in a method of determining the phase of an SPP with respect to the phase of the reflected laser beam which acts as an intrinsic reference:

$$\phi = \cos^{-1}\left(\frac{I_s - I_s^{\text{scat}} - I_s^{\text{spp}}}{2\sqrt{I_s^{\text{scat}} I_s^{\text{spp}}}}\right). \quad (6)$$

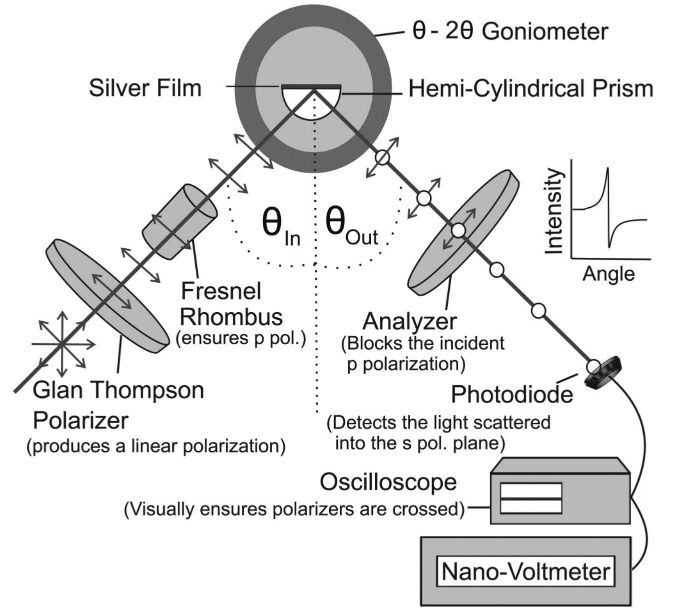

FIG. 4. Placing an analyzer in the reflection channel of a modified ATR setup to block the reflected p-polarized light and accurately recording the orthogonally scattered light produces a phase-related intensity line shape.

III. EXPERIMENTAL METHODS

While the method is not limited to a specific SPP excitation geometry, the experimental setup chosen here for the phase intensity measurements is similar to that employed in regular theta/two-theta angular interrogation Kretschmann configurations but with the sole addition of an analyzer polarizer in the reflection channel. It is thus an ellipsometric setup similar to the one used by Naraoka and Hooper [29,30]. However, in this case, the analyzer is employed to filter out the reflected p-polarized light, leaving the nonplane-of-incidence polarized scattered light.

Two distinct wavelengths of visible illumination have been used to characterize the signal. In the present study the wavelengths employed are $\simeq$790 nm (Ti-Sapphire laser in CW mode, Griffin C, KM Labs) and 561.2 nm (single mode stabilized diode laser, Torus, Oxius).

As illustrated in the experimental setup in Fig. 4, the incident beam is passed through a high grade Glan-Thompson polarizer (B. Halle, PGT 2.10 + PGT 0.8) which has an exceptional extinction ratio of 10^{-8}. The Glan-Thompson polarizer is employed to improve the linear polarization ratio of the incident laser sources and to precisely define its polarization orientation. The incident beam is then passed through a double Fresnel rhombus (B. Halle, RFR 1.500), which allows the incident linear polarization to be freely rotated to ensure a strict incident p polarization. A number of fine adjust micrometer slits are used to constrain the beam and to improve the collimation, as a very small spot size is important for angular

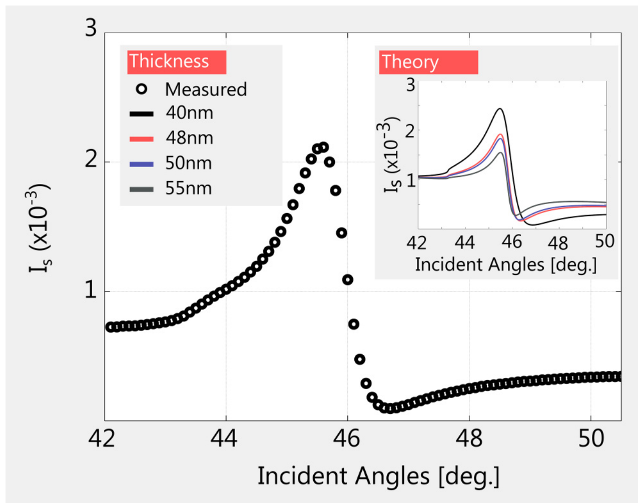

FIG. 5. Direct measurement of the s-polarization intensity in the reflection channel of an ATR configuration illuminated with p-polarized light. Sample is 43 nm of silver on a Fused silica prism. The insert shows theoretical prediction from cross-polarization scattering model at various thicknesses.

resolution considerations relating to plasmon excitation. On reflection from the prism/metal interface, the reflected light is passed through a second identical high grade Glan-Thompson analyzer polarizer. The signal is passed though a final micrometer slit and the resulting photodiode (BPW34) measurement is recorded using a Nano-Voltmeter (Agilent, 34420 A).

All angular scans correspond to going from lower momentum to higher momentum(e.g., $40^\circ \rightarrow 50^\circ$), with 0° being normal to the surface. When performing conventional angular SPR reflectivity scans no analyzer is present. For phase measurements, the Glan-Thompson analyzer is always orientated perpendicularly to the incident polarization. Due to the high quality of the polarizers only the intensity of the s-polarized components are detected in the reflection channel.

Silver (Goodfellow, 99.99%) thin films are deposited by vacuum thermal evaporation directly onto both BK7 and fused silica prisms. Base pressures are typically 5×10^{-5} mbar.

IV. EXPERIMENTAL RESULTS AND DISCUSSION

Multiple samples were used with varying thicknesses in order to illustrate the generality of the model over the entire region of SPP excitation. All samples were mounted in the system shown in Fig. 4 with the incoming polarization set to p polarization; both angle-dependent intensities of the resultant p-polarized and s-polarized reflected lights were recorded consecutively. Figure 5 shows the directly reflected intensity of s-polarized light. An example of the classically measured p-polarization signal is shown in Fig. 1(a). From these two measurements alone, which only require an additional quality polarizer in the setup, the roughness parameters, Gaussian width (ω), and cross-polarization scattering probability ($C'_{p\rightarrow s}$) can be determined. Table I shows these variables extracted from such pairs of measurements in conjunction with Eqs. (2) and (3) for four distinct thicknesses of silver films on Fused Silica prisms. Each value is specific to the

TABLE I. Roughness parameters for silver film samples $1-4$; ω is the Gaussian width from (1) and $C'_{p\rightarrow s}$ is the likelihood of cross-polarization scattering to occur used as the proportionality constant of Eqs. (2) and (3).

Sample	Thickness (nm)	ω (deg.)	$C'_{p\rightarrow s}(\times 10^{-3})$
1	43	0.1701	0.8220
2	56	0.1261	2.0836
3	70	0.2240	3.4855
4	75	0.1477	2.4636

sample and is a consequence of the manufacturing procedure, environmental history, and the thickness-dependent angle under which the SPP maximum (and related features) occurs. From these values, along with the Fresnel prediction of the reflectivity, R_n^B can be determined. Consequently, the phase shift between the two channels can be measured and then directly calculated from Eq. (6) which is the main result of this article. Figure 6 demonstrates the high quality of the method presented here of determining the SPP phase with respect to the reflected laser beam from the cross-polarization scattered light as it compares our measured data directly with the theoretical predictions. The agreement between the measurements (open circles) and the theoretical calculations (solid lines) is stunning—especially if one takes into account that, despite all efforts, the measured data must have some residual noise (e.g., originating from laser intensity fluctuations, dust particles in the laser beam, and changes in laser pointing) and the fact that the theoretical predictions must assume a certain simplified roughness distribution (Gaussian) which is a good approximation but in no way identical to the roughness on our samples. Along with determination of the phase, shown in Fig. 6, the direct measurement itself can be utilized for local refractive index-sensitive systems. The sensitivity of such systems depends on how steep the phase changes are for a given angular change. An excellent measure for this is the angular separation of the minimum and maximum of the phase. Figure 7 shows

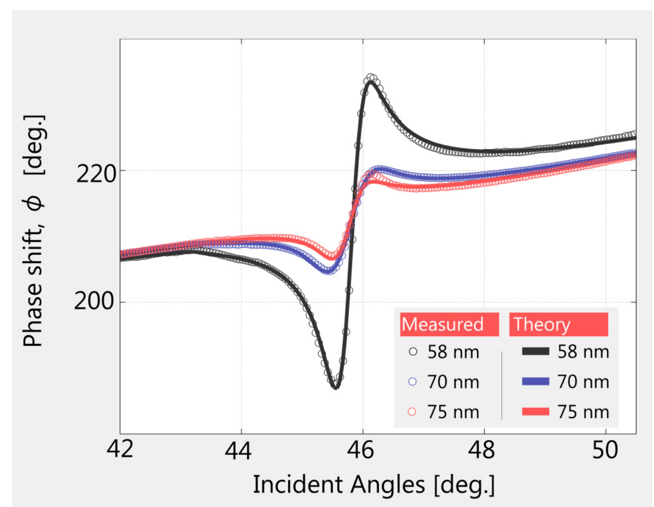

FIG. 6. Angular-dependent phase calculation from Eq. (6). Silver films on fused silica prism with $\lambda = 561$ nm.

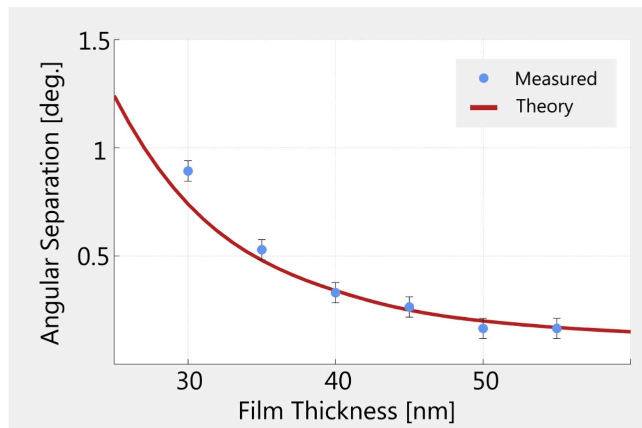

FIG. 7. Calculated and measured maximum to minimum separation distance for $\lambda = 790$ nm incident silver films through BK7.

the angular separation of the maximum and minimum phase points of the systems investigated, taken from measurements performed at a wavelength of 790 nm. The change in wavelength has deliberately been made to illustrate the versatility of the method—not only extending it to different thicknesses as shown above but also demonstrating that it can be used with arbitrary wavelengths. There is a clear trend in the narrowing of the feature as is indicated by both the theoretical and the experimental values. The angular separation of maximum and minimum values sharpens as the metal becomes thicker until it reduces to a relatively stable value of roughly 0.2°. Significantly, the optimum SPP excitation thickness has no effect on the measured signal. This is primarily because the *s*-polarization signal, I_s, is strongly dependent on the cosine of the phase shift rather than the phase shift directly. This is seen as the strong dominance of the phase term, $\cos(\phi)$, in Eq. (4) in comparison with the intensity terms.

One critical remark would be to note that the predictions and measurements of the angular separation work well for all thicknesses and are within the error bars but for the thinnest system investigated at 30 nm thickness. A potential reason for this deviation might be that the expected Gaussian distribution of roughness is perturbed for ultrathin metal films on substrates like quartz as the initial growth mode of the coinage metal would typically deviate from its bulk growth mode because of the nonmatching lattice constants between the substrate and its coating. In this vein, this is not a failure of the predictions but aids in analyzing the deviations in growth mode for thin films when compared against the expected distribution.

V. CONCLUSIONS

The cross-polarization scattering model, in conjunction with surface roughness-induced Gaussian broadening, can be utilized to determine the phase of the SPP phenomenon. Through two standard measurements the model illustrates a straightforward approach to phase retrieval. The angular dependence for three samples of varying thicknesses is calculated and shown to accurately reflect the phase values predicted by a Gaussian-broadened version of Fresnel equations; see Fig. 6.

In addition to phase calculations, the signal detected directly in the *s*-polarization configuration (I_s) has a strong metal thickness dependence and itself has the potential to be utilized within local refractive index sensor technologies.

ACKNOWLEDGMENTS

The authors acknowledge the Science Foundation Ireland for awarding the Future Innovator Prize (SFI 18/FIP/3551R), the Research Frontier project (SFI 11/RFP/MTR 3113), and the Irish Research Council (IRC).

[1] E. Kretschmann and H. Raether, Radiative decay of nonradiative surface plasmons excited by light, Z. Naturforsch. A **23**, 2135 (1968).
[2] J. Homola, *Surface Plasmon Resonance Based Sensors* (Springer, Berlin, Heidelberg, 2006)
[3] K. Kneipp, Y. Wang, H. Kneipp, L. T. Perelman, I. Itzkan, R. R. Dasari, and M. S. Feld, Single Molecule Detection Using Surface-Enhanced Raman Scattering (SERS), Phys. Rev. Lett. **78**, 1667 (1997).
[4] I. Gryczynski, J. Malicka, K. Nowaczyk, Z. Gryczynski, and J. R. Lakowicz, Effects of sample thickness on the optical properties of surface plasmon-coupled emission, J. Phys. Chem. B **108**, 12073 (2004).
[5] D. Zerulla, G. Isfort, M. Kölbach, A. Otto, and K. Schierbaum, Sensing molecular properties by atr-spp raman spectroscopy on electrochemically structured sensor chips, Electrochim. Acta **48**, 2943 (2003).
[6] A. P. Hibbins, B. R. Evans, and J. R. Sambles, Experimental verification of designer surface plasmons, Science **308**, 670 (2005).
[7] S. I. Bozhevolnyi, V. S. Volkov, E. Deveaux, J. Y. Laluet, and T. W. Ebbesen, Channel plasmon subwavelength waveguide components including interferometers and ring resonators, Nature (London) **440**, 508 (2006).
[8] S. Y. Wu, H. Ho, W. C. Law, C. Lin, and S. K. Kong, Highly sensitive differential phase-sensitive surface plasmon resonance biosensor based on the mach-zehnder configuration, Opt. Lett. **29**, 2378 (2004).
[9] A. V. Kabashin and P. I. Nikitin, Interferometer based on a surface-plasmon resonance for sensor applications, Quantum Electron. **27**, 653 (1997).
[10] F. Abelès, Surface electromagnetic waves ellipsometry, Surf. Sci. **56**, 237 (1976).
[11] A. V. Kabashin, S. Patskovsky, and A. N. Grigorenko, Phase and amplitude sensitivities in surface plasmon resonance bio and chemical sensing, Opt. Express **17**, 21191 (2009).
[12] S. Shen, T. Liu, and J. Guo, Optical phase-shift detection of surface plasmon resonance, Appl. Opt. **37**, 1747 (1998).
[13] T. König, M. Weidemüller, and A. Hemmerich, Real-time phase-shift detection of the surface plasmon resonance, Appl. Phys. B **93**, 545 (2008).

[14] B. Ran and S. G. Lipson, Comparison between sensitivities of phase and intensity detection in surface plasmon resonance, Opt. Express **14**, 5641 (2006).

[15] V. E. Kochergin, A. A. Beloglazov, M. V. Valeiko, and P. I. Nikitin, Phase properties of a surface-plasmon resonance from the viewpoint of sensor applications, Quantum Electron. **28**, 444 (1998).

[16] A. V. Kabashin, V. E. Kochergin, and P. I. Nikitin, Surface plasmon resonance bio- and chemical sensors with phase-polarisation contrast, Sens. Actuators B Chem **54**, 51 (1999).

[17] X. L. Yu, D. X. Wang, X. Wei, D. Xiang, L. Wei, and Z. Xinsheng, A surface plasmon resonance imaging interferometry for protein micro-array detection, Sens. Actuators B Chem **108**, 305 (2005).

[18] Y. D. Su, S. J. Chen, and T. L. Yeh, Common-path phase-shift interferometry surface plasmon resonance imaging system, Opt. Lett. **30**, 1488 (2005).

[19] S. Crosbie, E. McClean, and D. Zerulla, Polarization dependant scattering as a tool to retrieve the buried phase information of surface plasmon polaritons, Appl. Phys. Lett. **101**, 161603 (2012).

[20] Y. H. Huang, H. P. Ho, S. Y. Wu, and S. K. Kong, Detecting phase shifts in surface plasmon resonance: A review, Adv. Opt. Tech. **2012**, 471957 (2012).

[21] S. J. Elston and J. R. Sambles, Polarization conversion using prism-coupled surface plasmon-polaritons, J. Mod. Opt. **38**, 1223 (1991).

[22] A. A. Maradudin, *Light Scattering and Nanoscale Surface Roughness* (Springer, Boston, MA, 2007).

[23] P. Hermansson, G. Forssell, and J. Fagerström, *A Review of Models for Scattering from Rough Surfaces* (Swedish Defence Research Agency, Linköping, 2003).

[24] T. A. Germer, *Measuring Interfacial Roughness by Polarized Optical Scattering, in Light Scattering and Nanoscale Surface Roughness. Nanostructure Science and Technology,* edited by A. A. Maradudin (Springer, Boston, MA, 2007).

[25] A. A. Maradudin and E. R. Méndez, Light scattering from randomly rough surfaces, Sci. Prog. **90**, 161 (2007).

[26] G. Isfort, K. Schierbaum, and D. Zerulla, Causality of surface plasmon polariton emission processes, Phys. Rev. B **73**, 033408 (2006).

[27] G. Isfort, K. Schierbaum, and D. Zerulla, Polarization dependence of surface plasmon polariton emission, Phys. Rev. B **74**, 033404 (2006).

[28] B. Ashall, M. Berndt, and D. Zerulla, Tailoring surface plasmon polariton propagation via specific symmetry properties of nanostructures, Appl. Phys. Lett. **91**, 203109 (2007).

[29] R. Naraoka and K. Kajikawa, Phase detection of surface plasmon resonance using rotating analyzer method, Sens. Actuators B Chem **107**, 952 (2005).

[30] I. R. Hooper and J. R. Sambles, Sensing using differential surface plasmon ellipsometry, J. Appl. Phys. **96**, 3004 (2004).